Metal–Organic Frameworks

DOI: 10.1002/anie.201103265

A Multiferroic Perdeutero Metal–Organic Framework**

Da-Wei Fu, Wen Zhang, Hong-Ling Cai, Yi Zhang, Jia-Zhen Ge, Ren-Gen Xiong,* Songping D. Huang, and Takayoshi Nakamura*

Recently, very intensive research interests have focused on the exploration of metal-organic frameworks (MOF) as potential ferroelectrics and multiferroics, which exhibit the coexistence of magnetic and ferroelectric ordering.[1–6] One example is the class of MOFs with the formula [{cationic guest molecule}{(metal ion)(formate)$_3$}],[1–4] which closely resemble pure inorganic ferroelectric $BaTiO_3$ and multiferroic $BiFeO_3$ with perovskite ABO_3-type structures in which A is the cationic guest molecule, the B is the metal ion, and the anion O is replaced by formate.

It is known that most ABO_3-type perovskite compounds display sequential structural phase transitions.[7] For example, $BaTiO_3$ exhibits three structural phase transitions: a paraelectric–ferroelectric transition at 393 K (cubic *m*3*m* to tetragonal 4*mm* phase), a ferroelectric–ferroelectric transition at 278 K (tetragonal 4*mm* to orthorhombic *mm*2 phase), and a ferroelectric–ferroelectric transition at 180 K (orthorhombic *mm*2 to rhombohedral 3*m* phase). A similar sequence is also found in $KNbO_3$, that is, a polar tetragonal phase between 498 and 708 K, an orthorhombic phase between 263 and 498 K, and a rhombohedral phase below 263 K. For comparison, the recently reported MOFs based on metal formate as anionic frameworks all display only one structural phase transition with low-temperature magnetic ordering. Pioneering work on magnetic properties, dielectric behaviors, and ferroelectric explorations of metal formates has been done by the groups of Wang and Gao,[4] Kobayashi,[1] and Cheetham.[2] To our knowledge, no structural phase transition above room temperature has been reported for these metal formates, although Kobayashi and co-workers have investigated the effect of deuteration of the neutral guest molecules in MOF [Mn_3(formate)$_6$], which did not result in a structural phase transition above room temperature.[1]

Guest molecules undergoing order–disorder motions are responsible for the inducement of (or are the driving force for) structural phase transitions, which are probably distinct from hydrogen-related order–disorder motions. Usually, replacement of a hydrogen atom by a deuterium atom results in two significant changes in physical properties: 1) sharp enhancement of phase-transition temperature (T_C), such as in the ferroelectric compounds KH_2PO_4 and KD_2PO_4 with $\Delta T_C \approx 90$ K and antiferroelectric compounds $NH_4H_2PO_4$ and $ND_4D_2PO_4$ with $\Delta T_C \approx 94$ K; 2) enhancement of the dielectric constant by one to two orders of magnitude or striking enhancement of the saturated polarization (P_s). Consequently, molecules or cations confined in cage-like frameworks probably only display order–disorder features like the typical ferroelectric $NaNO_2$, even if the disordered atoms are bonded to H atoms. To testify this assertion, it is very important and interesting to explore perdeutero MOFs to see how deuteration affects T_C and the dielectric constant, that is, the isotopic effect. Encouraged by pioneering work on the system $[Cu(HCOO)_2]\cdot 4H_2O/[Cu(HCOO)_2]\cdot 4D_2O$,[8] we carried out synthesis, variable-temperature crystal-structure determinations, thermal properties measurements including differential scanning calorimetry (DSC) and specific heat capacity (C_p), and dielectric constant measurements with or without magnetic field on the system [{$(CD_3)_2ND_2$}Co(DCOO)$_3$] (PD-DMACoF, where PD-DMA = perdeuterodimethylammonium and DCOO = perdeuteroformate). Surprisingly, there is a new phase transition above room temperature at about 319 K as well as a low-temperature structural phase transition, in contrast to [{$(CH_3)_2NH_2$}Co(HCOO)$_3$] (DMACoF) with only one $T_C = 155$ K. More interestingly, the dielectric constant of PD-DMACoF displays a significant Debye relaxation like the typical order–disorder-type ferroelectric $NaNO_2$.

Electrospray mass spectrometry (ES-MS) of the extraction solution of PD-DMACoF destroyed by ethylenediaminetetraacetic acid displays a peak at *m*/*z* 54.11, assigned to the perdeutero dimethylammonium ion (Figure 1). Crystal-structure determination of PD-DMACoF clearly reveals that the PD-DMA cation at the center of the ReO_3-type cavity is disordered at room temperature (phase II, 185–319 K), with

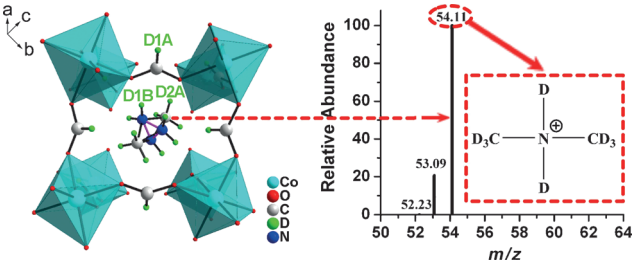

Figure 1. Cage-like 3D framework of PD-DMACoF and its ES mass spectrum.

[*] D.-W. Fu, Prof. W. Zhang, Dr. H.-L. Cai, Dr. Y. Zhang, Dr. J.-Z. Ge, Prof. R.-G. Xiong, Prof. S. D. Huang, Prof. T. Nakamura
Ordered Matter Science Research Center, Southeast University
Nanjing 211189, P.R. China
E-mail: zhangwen@seu.edu.cn
xiongrg@seu.edu.cn

[**] This work was supported by the National Natural Science Foundations of China (21071030, 20931002, and 90922005) and the 973 project (2009CB6232003). X.R.G. thanks the Japanese Government for a JSPS fellowship, Joint NSFC–JSPS 21111140013 to X.R.G. and Prof. Takayoshi Nakamura (Hokkaido University) and the NSFC for a grant (20540420518) to X.R.G. and Prof. Songping D. Huang (Kent State University).

Supporting information for this article is available on the WWW under http://dx.doi.org/10.1002/anie.201103265.

the nitrogen atom distributed over three equivalent positions as in the analogous DMACoF system.[9] There are disordered deuterium bonds between the deuterium atoms of the ND_2 group and the oxygen atoms of the formate framework (N···O ca. 2.919 Å), similar to that of DMACoF. A similar situation is found in the high-temperature phase (phase I, above 319 K), in which the nitrogen atom is distributed over three equivalent positions. However, in the low-temperature phase (phase III, below 185 K) the nitrogen atom is disordered over two equivalent positions, as symmetry-breaking occurs during the cooling process from the trigonal (space group $R\bar{3}c$, No. 167, 12 symmetric elements E, $2\,C_3$, $3\,C_2$, i, $2\,S_6$, and $3\,\sigma_v$) to the monoclinic crystal system (space group Cc, two symmetric elements E and σ_h), corresponding to the disappearance of 10 symmetric elements with an Aizu notation of $\bar{3}mFm$. This monoclinic system is a typical ferroelectric with three polarization directions. Furthermore, we can clearly observe the changes associated with the symmetry-breaking phenomenon from spatial symmetry operations as shown in Scheme S1 in the Supporting Information.

As expected, ferroelectrics all display a second harmonic generation (SHG) effect, which is very sensitive to the symmetry-breaking occurring during temperature changes, because only noncentrosymmetric solids display SHG signals. At the same time, this technology is widely used for the confirmation of symmetry-breaking and ferroelectric domain detection in ceramic ferroelectrics.[11] To our knowledge, there are no documents regarding the relationship between symmetry-breaking and SHG signal for molecule-based ferroelectrics. The temperature dependence of the SHG signal of PD-DMACoF depicted in Figure 2 clearly shows that the SHG effect appears below T_C (ca. 151 K), a good agreement

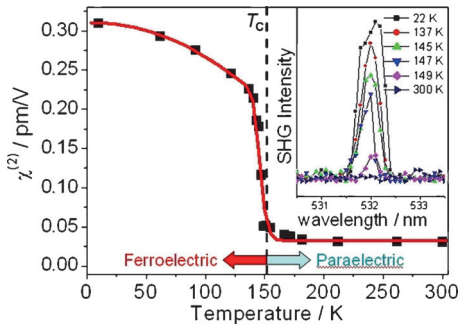

Figure 2. Temperature dependence of the second-order nonlinear effective coefficient. The inset shows the intensity of SHG as a function of wavelength at different temperatures.

with the low-temperature crystal-structure determination. However, between 151 and 319 K, and above 319 K, no SHG signal is observed, suggesting that in these temperature ranges the solid-state structure is centrosymmetric, also in good agreement with crystal-structure determinations.

DSC measurement is a common method for detecting whether a phase transition occurs in response to external temperature stimulus. In the case of PD-DMACoF, there is a heat anomaly at approximately 159 K upon warming and 151 K upon cooling (Figure 3). The relatively large thermal

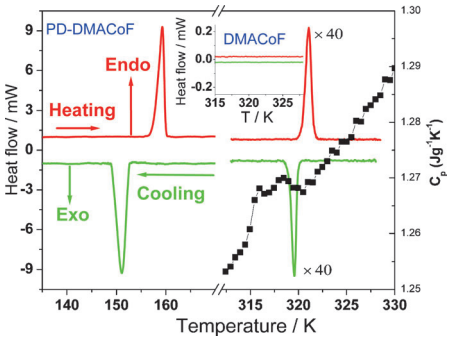

Figure 3. DSC curves of PD-DMACoF at low and high temperatures. The inset shows DSC curves of DMACoF at high temperature. The black squares (right) show the heat capacity of PD-DMACoF as a function of temperature. Note that the heat flow at high temperature is enlarged by a factor of 40 for clarity.

hysteresis of 8 K and a sharp peak indicates a reversible first-order phase transition. Interestingly, there is also a heat anomaly above room temperature, appearing at approximately 319 K upon cooling and 321 K upon heating, with a small thermal hysteresis of 2 K, probably indicating a reversible second-order phase transition. In comparison, the non-deuterated sample DMACoF does not display a heat anomaly above room temperature (inset of Figure 3). Furthermore, the C_p curve may confirm the phase transition and its type. Figure 3 clearly shows that a round peak appears at approximately 316–319 K, confirming that the phase transition is a typical second-order one, like that of triglycine sulfate (TGS). Thus, the deuteration-induced phase transition is similar to the case found in the $DCrO_2/HCrO_2$ system, in which $HCrO_2$ fails to display a phase transition while $DCrO_2$ clearly exhibits a structural phase transition after deuteration.[10]

Entropy change (ΔS) at the phase transition depends significantly on the choice of the baseline. From our structural studies, the PD-DMA cation is strongly disordered in the room- and high-temperature phases. Knowing that the changes in entropy accompany the two phase transitions, it is possible to find the number of distinguishable positions of the cation from $\Delta S = R\ln(N2/N1)$ where $N1$ and $N2$ are the numbers of distinguishable positions of the PD-DMA cation in the ordered and disordered phases. As the DSC results show two phase transitions, the total change in entropy is the sum of the changes at the two temperatures, $\Delta S = \Delta S_{T1} + \Delta S_{T2}$, where $T1 = 159$ K, $T2 = 319$ K, $\Delta S_{T1} = \Delta H/T1 = 4.42\ \mathrm{J\,mol^{-1}\,K^{-1}}$, and $\Delta S_{T2} = = 0.06\ \mathrm{J\,mol^{-1}\,K^{-1}}$. The total entropy change found experimentally at these two phase transitions is close to $\Delta S \approx 4.48\ \mathrm{J\,mol^{-1}\,K^{-1}}$, indicating that these transitions are of the order–disorder type ($N2/N1 \approx 3{:}2$). The entropy change around $T1$ is nearly 99% of the total entropy change, and the entropy change around $T2$ is negligibly small. The value of ΔS_{T1} is close to the theoretically predicted value of $R\ln(2) = 5.06\ \mathrm{J\,mol^{-1}\,K^{-1}}$. Given that in the low-temperature ordered phase III the PD-DMA cation is partially ordered and there are two possible position of the PD-DMA cation ($N1 = 2$) and in the disordered phase II there are three distinguishable positions of the PD-DMA

cation ($N2=3$), $\Delta S = R\ln(3/2)$. The above conclusions are confirmed by the crystal structures of all three phases. In the room-temperature phase II, PD-DMA can take three positions as a result of atom disordering and reorientation around the pseudo-threefold axis of the N atom, while in the low-temperature phase III, the N atom takes two possible positions.

As mentioned above, the physical properties will sharply change near the phase-transition point, and the magnitude of the changes will be relative to the characteristics of the phase transitions, that is, common phase transition, ferroelastic transition, or ferroelectric transition. Both DSC and C_p curves indicate that there is a phase transition at about 320 K and no dielectric anomaly in the temperature range of 275–350 K (Figure S1 in the Supporting Information). This finding indicates that the phase transition of PD-DMACoF is probably due to a nonpolar soft mode without dielectric constant anomaly like that of $SrTiO_3$, which is also in agreement with the measurement of the temperature dependence of the SHG effect. However, it is very interesting to note that the real part (ε') of the complex dielectric constant ($\varepsilon = \varepsilon' - i\varepsilon''$) of PD-DMACoF displays a broad peak at 170 K at 1 KHz and at 250 K at 1 MHz (Figure 4). It shows a very large relaxation, with a difference of approximately 80 K from low frequency to high frequency. The maximum value of the dielectric constant decreases gradually with increasing frequency. The frequency dependence of the dielectric constant shows a typical character of diffusion transitions and dielectric relaxation.

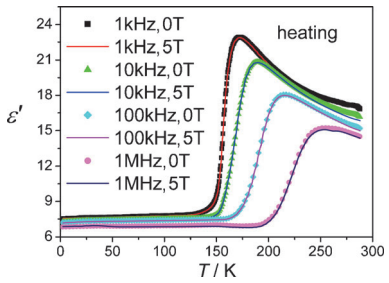

Figure 4. The real part of the complex dielectric constants of PD-DMACoF measured at different frequencies with and without a magnetic field of 5 T approximately along the *a* axis.

Furthermore, the real part of the dielectric constant of the polycrystalline samples of PD-DMACoF approximately doubles in the warming process from the low temperature to T_C. The base value is about 6.5–8 and the peak value is of about 16–23 in a frequency range of 1 KHz to 1 MHz, suggesting this phase transition may be improper ferroelectric with a step-like dielectric enhancement. When a 5 T magnetic field is applied, the dielectric constants are unchanged, which hints that there is no coupling between magnetization and polarization. Notably, no H-atom isotopic effect is observed ($\Delta T_C \approx 1$ K), suggesting that the nature of the phase transition should be purely disorder–order-type, like the case of $NaNO_2$.

To test this point, it is necessary to discuss the frequency dependence of the complex dielectric permittivies (Figure 5).

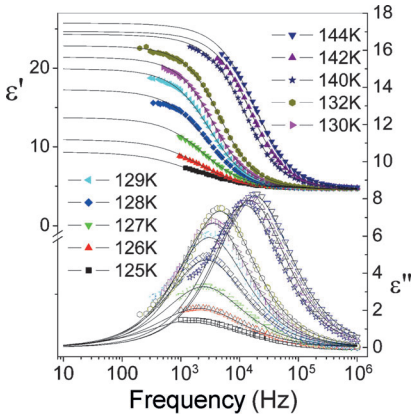

Figure 5. The frequency dependence of the complex dielectric permittivities of PD-DMACoF approximately along the *a* axis. ε' filled symbols, ε'' open symbols.

The real part ε' gradually decreases with increasing frequency. The imaginary part ε'' as a function of alternating-current (ac) frequency exhibits a broad peak just where the ε' drops most steeply. This behavior is characteristic of a Debye-like dielectric relaxation, in which the reorientation of dipoles cannot respond to the applied ac electric field when high frequency exceeds a relaxation rate $1/\tau$. This mechanism is expressed in Equation (1):

$$\varepsilon = \varepsilon_\infty + \frac{\varepsilon_s - \varepsilon_\infty}{1 + (i\omega\tau)^\alpha}$$

$$\varepsilon' = \varepsilon_\infty + \frac{(\varepsilon_s - \varepsilon_\infty)(1 + \cos\frac{\alpha\pi}{2}\omega^\alpha\tau^\alpha)}{1 + 2\cos\frac{\alpha\pi}{2}\omega^\alpha\tau^\alpha + \omega^{2\alpha}\tau^{2\alpha}} \quad (1)$$

$$\varepsilon'' = \frac{(\varepsilon_s - \varepsilon_\infty)\sin\frac{\alpha\pi}{2}\omega^\alpha\tau^\alpha}{1 + 2\cos\frac{\alpha\pi}{2}\omega^\alpha\tau^\alpha + \omega^{2\alpha}\tau^{2\alpha}}$$

where τ is the relaxation time, ω is the angular frequency, α is the distribution of relaxation times, and ε_s and ε_∞ are the static and high-frequency dielectric constants, respectively. A plot of $\varepsilon''(\omega)$ versus $\varepsilon'(\omega)$ at a given temperature results in a curve fitted as an arc of a circle. For a single relaxation, the points (ε', ε'') lie on a semicircle centered at $((\varepsilon_s + \varepsilon_\infty)/2, 0)$ and intersecting the ε' axis at ε_s and ε_∞ (Cole–Cole plot, Figure 6). The relaxation frequency $1/(2\pi\tau)$ was obtained from the data fitted at temperatures above T_C (ca. 151 K). It is proportional to $(T - T_C)$ near T_C and bends upward far above T_C, showing that near T_C the present case displays a "classical" critical slowing of the relaxation frequency within about 10 K around T_C in the paraelectric phase.[11a] From the Arrhenius equation ($\tau = \tau_0 \exp(E_a/k_B T)$), the activity energy E_a and relaxation time τ_0 are calculated to be 464 J mol^{-1} and 1.02×10^{-15} s, respectively. Very similar dielectric behaviors are observed as the critical slowing-down in typical order–disorder-type ferroelectrics such as $NaNO_2$.[11] For PD-DMACoF, the overall relaxation rate is two to three orders of magnitude slower than that of $NaNO_2$, similar to that found in [{H_2-TPPZ}{Hba}$_2$] (TPPZ = 2,3,5,6-tetra(2′-pyridyl)pyrazine, H_2ba = bromanilic acid) and pyrazinium tetrafluoroborate.[12]

Finally, the good dielectric hysteresis loop as shown in Figure 7 a is a very strong evidence that the PD-DMACoF is a

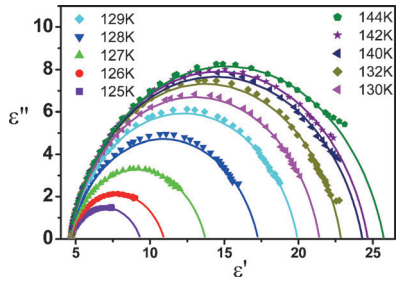

Figure 6. The Cole–Cole diagram of PD-DMACoF.

relaxation-type ferroelectric with a saturation polarization of ca. 1.04 $\mu C cm^{-2}$, much higher than that of Rochelle salt (0.2 $\mu C cm^{-2}$), much smaller than that of TGS (3.5 $\mu C cm^{-2}$), and comparable to that of $[NH_4][Zn(HCOO)_3]$ (1.0 $\mu C cm^{-2}$). When an external electric field applied, the Gibbs free energy should be written as in Equation (2):

$$G_1 = G_0 + \frac{1}{2}AP_x^2 + \frac{1}{4}CP_x^4 + \frac{1}{6}FP_x^6 - EP_x \quad (2)$$

where E is the applied electric field, A, C and F are the coefficients, and P_x is the polarization along the a axis. Thus, the free energy reaches its extreme value when [Eq. (3)]:

$$\partial G_1/\partial P_x = AP_x + CP_x^3 + FP_x^5 - E = 0 \quad (3)$$

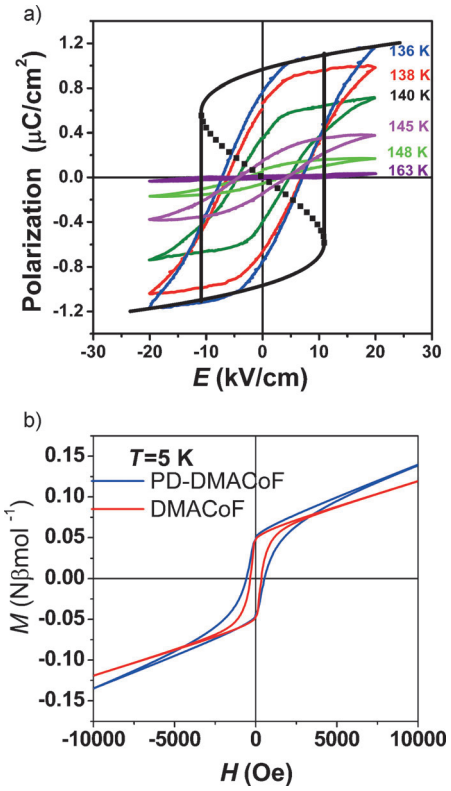

Figure 7. a) The dielectric hysteresis loop recorded just below T_C (ca. 151 K). The frequency is fixed at 50 Hz approximately along the a axis. The black solid line shows the fitted hysteresis loop according to Landau theory. b) The magnetic hysteresis loop at 5 K for PD-DMACoF (blue) and DMACoF (red) as a reference.[4]

The fitted hysteresis loops are shown in Figure 7a by black solid lines, which are consistent with the experimental results.

Furthermore, as expected, PD-DMACoF displays a perfect magnetic hysteresis loop at 5 K (Figure 7b). Owing to the absence of magnetically induced dielectric anomaly (Figure 4), PD-DMACoF should be a ferromagnetic ferroelectric without coupling of magnetism and electricity. However, it is still very important that PD-DMACoF is a very rare example of a single-phase relaxation-type multiferroic MOF, which would find applications in molecule-based electronics in future.[13e]

According to Landau theory, the Gibbs free energy for magnetoelectric system can be written as Equation (4):

$$G(E,H) = G_0 - P_i^s E_i - M_i^s H_i - \frac{1}{2}\varepsilon_0\varepsilon_{ij}E_iE_j - \frac{1}{2}\mu_0\mu_{ij}H_iH_j - \alpha_{ij}E_iH_j - \frac{1}{2}\beta_{ijk}E_iH_jH_k - \frac{1}{2}\gamma_{ijk}H_iE_jE_k \quad (4)$$

where G_0 is the ground state free energy, subscripts (i, j, k) refer to the three components of a variable in spatial coordinates, E_i and H_i are the components of the electric field E and magnetic field H, respectively, P_i^s and M_i^s are the components of spontaneous polarization P_s and magnetization M_s, ε_0 and μ_0 are the dielectric permeability and magnetic susceptibility of vacuum, ε_{ij} and μ_{ij} are the second-order tensors of dielectric permeability and magnetic susceptibility, β_{ijk} and γ_{ijk} are the third-order tensor coefficients and, most importantly, α_{ij} is the component of a tensor which is designated as the linear magnetoelectric effect and corresponds to the induction of a polarization by a magnetic field or a magnetization by an electric field. The rest of the terms in the preceding equations correspond to the high-order magnetoelectric effects parameterized by tensors β and γ. Then the polarization is given in Equation (5):

$$P_i(E,H) = -\frac{\partial G}{\partial E_i} = P_i^s + \varepsilon_0\varepsilon_{ij}E_j + \alpha_{ij}H_j + \frac{1}{2}\beta_{ijk}H_jH_k + \gamma_{ijk}H_iE_j \quad (5)$$

and the magnetization is given in Equation (6):

$$M_i(E,H) = -\frac{\partial G}{\partial H_i} = M_i^s + \mu_0\mu_{ij}H_j + \alpha_{ij}E_j + \beta_{ijk}E_iH_j + \frac{1}{2}\gamma_{ijk}E_jE_k \quad (6)$$

Unfortunately, the magnetoelectric effect in single-phase compounds is usually too small to be practically applicable. In our case, there is no magnetoelectric coupling effect, so α, β and γ are zero.

DSC, specific heat capacity, and dielectric measurements have successfully demonstrated that the perdeutero MOF PD-DMACoF undergoes two phase transitions, including one above room temperature, which is unprecedented in the known metal formates. The dielectric properties between phase II and phase III are reported for the first time to exhibit a typical relaxation behavior, like that of $NaNO_2$, which is an order–disorder-type ferroelectric. The magnetic and dielectric hysteresis loops indicate that PD-DMACoF is both ferromagnetic and ferroelectric. The results herein should shed light on the exploration of MOF-based relaxor ferroelectrics.[13]

Experimental Section

PD-DMACoF was prepared under solvothermal conditions at 413 K. A Pyrex tube (ca. 18 cm with an inner diameter of 1.3 cm) containing a solution of 50 vol% PD-DMF [$(CD_3)_2NCDO$] in D_2O (2 mL) was charged with $CoCl_2$ (0.5 mmol). The solution was frozen by liquid nitrogen and the tube was flame-sealed. The sealed tube was put in an oven at 413 K for four days and then cooled at a controlled rate. Pink-purple block crystals were obtained with a yield of about 70%. The phase purity of PD-DMACoF was confirmed by a good match of its powder XRD pattern with a simulation from the single-crystal structure determination (see the Supporting Information). X-ray diffraction was carried out on PD-DMACoF using a Rigaku CCD diffractometer with $Mo_{K\alpha}$ radiation. The structure of PD-DMACoF was solved by direct methods and refined by the full-matrix method based on F^2 using the SHELXL97 software package (Sheldrick, 1997). DSC measurements were performed on a PerkinElmer Diamond DSC instrument. Specific heat analyses were carried out on a Quantum Design PPMS apparatus. Complex dielectric permittivity was measured with an Agilent 4294A impedance analyzer. Dielectric hysteresis loops were recorded on a Radiant Precision Premier II and good loop curves were obtained by modification or compensation from subtracting paraelectric phase contributions, including dielectric and conductive (electric leakages) components. Although using pulse measurements (PUND pulse train technique) and pyroelectric measurements to check the reversal of the response signal with the reversal of polarization suggested by a referee, we still failed to obtain good dielectric hysteresis loops.

Received: May 12, 2011
Revised: August 29, 2011
Published online: October 25, 2011

Keywords: dielectrics · magnetic properties · organic–inorganic hybrid composites · phase transitions

[1] a) H.-B. Cui, B. Zhou, L.-S. Long, Y. Okano, H. Kobayashi, A. Kobayashi, *Angew. Chem.* **2008**, *120*, 3424 – 3428; *Angew. Chem. Int. Ed.* **2008**, *47*, 3376 – 3380; b) H.-B. Cui, Z.-M. Wang, K. Takahashi, Y. Okano, H. Kobayshi, A. Kobayashi, *J. Am. Chem. Soc.* **2006**, *128*, 15074 – 15075.

[2] a) P. Jain, N. S. Dalal, B. H. Toby, H. W. Kroto, A. K. Cheetham, *J. Am. Chem. Soc.* **2008**, *130*, 10450 – 10451; b) P. Jain, V. Ramachandran, R. J. Clark, H. D. Zhou, B. H. Toby, N. S. Dalal, H. W. Kroto, A. K. Cheetham, *J. Am. Chem. Soc.* **2009**, *131*, 13625 – 13627.

[3] M. Sánchez-Andújar, S. Presedo, S. Yáñez-Vilar, S. Castro-García, J. Shamir, M. A. Señarís-Rodríguez, *Inorg. Chem.* **2010**, *49*, 1510 – 1516.

[4] a) Z.-M. Wang, K.-L. Hu, S. Gao, H. Kobayashi, *Adv. Mater.* **2010**, *22*, 1526 – 1533; b) H.-L. Sun, Z.-M. Wang, S. Gao, *Coord. Chem. Rev.* **2010**, *254*, 1081 – 1100; c) K.-L. Hu, M. Kurmoo, Z.-M. Wang, S. Gao, *Chem. Eur. J.* **2009**, *15*, 12050; d) G.-C. Xu, X.-M. Ma, L. Zhang, Z.-M. Wang, S. Gao, *J. Am. Chem. Soc.* **2010**, *132*, 9588 – 9590.

[5] a) W. Zhang, H.-Y. Ye, H.-L. Cai, J.-Z. Ge, R.-G. Xiong, S. D. Huang, *J. Am. Chem. Soc.* **2010**, *132*, 7300 – 7300; b) W. Zhang, H.-Y. Ye, R.-G. Xiong, *Coord. Chem. Rev.* **2009**, *253*, 2980 – 2997; c) W. Zhang, Y. Cai, R.-G. Xiong, H. Yoshikawa, K. Awaga, *Angew. Chem.* **2010**, *122*, 6758 – 6760; *Angew. Chem. Int. Ed.* **2010**, *49*, 6608 – 6610; d) D.-W. Fu, W. Zhang, H.-L. Cai, Y. Zhang, J.-Z. Ge, R.-G. Xiong, K. Awaga, T. Nakamura, *J. Am. Chem. Soc.* **2011**, *133*, 12780 – 12786; e) H.-L. Cai, W. Zhang, J.-Z Ge, Y. Zhang, K. Awaga, T. Nakamura, R.-G. Xiong, *Phys. Rev. Lett.* **2011**, *107*, 147601 .

[6] a) W. Zhang, L.-Z. Chen, R.-G. Xiong, T. Nakamura, S. P. D. Huang, *J. Am. Chem. Soc.* **2009**, *131*, 12544 – 12545; b) H.-Y. Ye, D.-W. Fu, Y. Zhang, W. Zhang, R.-G. Xiong, S. P. D. Huang, *J. Am. Chem. Soc.* **2009**, *131*, 42 – 43; c) H.-Y. Ye, L.-Z. Chen, R.-G. Xiong, *Acta Crystallogr. Sect. B* **2010**, *66*, 387 – 395; d) T. Hang, W. Zhang, H.-Y. Ye, R.-G. Xiong, *Chem. Soc. Rev.* **2011**, *40*, 3577 – 3598.

[7] F. Jona, G. Shirane, *Ferroelectric Crystals*. Pergamon, New York, **1962**.

[8] K. Okada, H. Sugie, *J. Phys. Soc. Jpn.* **1968**, *25*, 1128 – 1132.

[9] Crystal data: Phase I ($T = 373$ K): $C_{15}Co_3D_{33}N_3O_{18}$, pink block, $0.3 \times 0.3 \times 0.2$ mm, $M_r = 753.43$, trigonal, $R\bar{3}c$, $a = b = 8.1980(10)$, $c = 22.268(5)$ Å, $\gamma = 120°$, $V = 1296.1(4)$ Å^3, $Z = 6$, $D_{calcd} = 1.931$ mg m^{-3}, $\mu = 1.986$ mm^{-1}, $S = 1.197$, $R(F) = 0.0247$, $wR(F^2) = 0.0713$. Phase II ($T = 273$ K): $C_{15}Co_3D_{33}N_3O_{18}$, pink block, $0.3 \times 0.3 \times 0.2$ mm, $M_r = 753.43$, trigonal, $R\bar{3}c$, $a = b = 8.2122(12)$, $c = 22.250(4)$ Å, $\gamma = 120°$, $V = 1299.5(4)$ Å^3, $Z = 6$, $D_{calcd} = 1.926$ mg m^{-3}, $\mu = 1.980$ mm^{-1}, $S = 1.188$, $R(F) = 0.0248$, $wR(F^2) = 0.0731$. Phase III ($T = 93$ K): $C_5CoD_{11}NO_6$, pink block, $0.3 \times 0.3 \times 0.2$ mm, $M_r = 251.14$, monoclinic, Cc, $a = 14.233(3)$, $b = 8.2037(16)$, $c = 8.8455(18)$ Å, $\beta = 122.79(3)°$, $V = 868.3(3)$ Å^3, $Z = 4$, $D_{calcd} = 1.921$ mg m^{-3}, $\mu = 1.976$ mm^{-1}, $S = 1.101$, $R(F) = 0.0508$, $wR(F^2) = 0.1299$. CCDC 795318, 795319, 795320 contain the supplementary crystallographic data for this paper. These data can be obtained free of charge from The Cambridge Crystallographic Data Centre via www.ccdc.cam.ac.uk/data_request/cif.

[10] T. Matsuo, T. Maekawa, A. Inaba, O. Yamamuro, M. Ohoma, M, Ichikawa, T. Tsuchida, *J. Mol. Struct.* **2006**, *790*, 129 – 134.

[11] a) G. Bator, R. Jakubas, *Phys. Status Solidi A* **1995**, *147*, 591; b) I. Hatta, *J. Phys. Soc. Jpn.* **1968**, *24*, 1043 – 1053.

[12] a) S. Horiuchi, R. Kumai, Y. Tokunaga, Y. Tokura, *J. Am. Chem. Soc.* **2008**, *130*, 13382 – 13391; b) A. Katrusiak, M. Szafraski, *J. Am. Chem. Soc.* **2006**, *128*, 15775 – 15785.

[13] a) S. Ohkoshi, H. Tokoro, T. Matsuda, H. Takahashi, H. Irie, K. Hashimoto, *Angew. Chem.* **2007**, *119*, 3302 – 3305; *Angew. Chem. Int. Ed.* **2007**, *46*, 3238 – 3241; b) A. Stroppa, P. Jain, P. Barone, M. Marsman, J. M. Perez-Mato, A. K. Cheetham, H. W. Kroto, S. Picozzi, *Angew. Chem.* **2011**, *123*, 5969; *Angew. Chem. Int. Ed.* **2011**, *50*, 5847 – 5850; c) G. Rogez, N. Viart, M. Drillon, *Angew. Chem.* **2010**, *122*, 1965 – 1967; *Angew. Chem. Int. Ed.* **2010**, *49*, 1921 – 1923; d) B. Zhou, A. Kobayashi, H.-B. Cui, L.-S. Long, H. Fujimori, H. Kobayashi, *J. Am. Chem. Soc.* **2011**, *133*, 5736 – 5739; e) G.-C. Xu, W. Zhang, X.-M. Ma, Y.-H. Chen, L. Zhang, H.-L. Cai, Z.-M. Wang, R.-G. Xiong, S. Gao, *J. Am. Chem. Soc.* **2011**, *133*, 14948 – 14951; f) C.-M. Liu, R.-G. Xiong, D.-Q. Zhang, D.-B. Zhu, *J. Am. Chem. Soc.* **2010**, *132*, 4044 – 4045; g) R. Samantaray, R. J. Clark, E. S. Choi, H. Zhou, N. S. Dalal, *J. Am. Chem. Soc.* **2011**, *133*, 3792 – 3795.

